energies

MDPI

Article

Parameterized Trajectory Optimization and Tracking Control of High Altitude Parafoil Generation

Xinyu Long, Mingwei Sun *, Minnan Piao and Zengqiang Chen

College of Artificial Intelligence, Nankai University, Tianjin 300350, China; longxinyu@mail.nankai.edu.cn (X.L.); piaominnan@mail.nankai.edu.cn (M.P.); chenzq@nankai.edu.cn (Z.C.)
* Correspondence: sunmw@nankai.edu.cn

Abstract: Parafoil trajectory directly affects the power generation of a high-altitude wind power generation (HAWPG) device. Therefore, it is particularly important to optimize the parafoil trajectory and then to track it effectively. In this paper, the trajectory of the parafoil at high altitudes is optimized and tracked in a comprehensively parameterized manner. Both the complex dynamic characteristics of the parafoil and the dexterous demand of the high-altitude controller are considered. Firstly, the trajectory variables and control signals are parameterized as Lagrange polynomials in terms of the corresponding values at the selected nodes. Then, the Radau pseudospectral method (PSM) is employed to reformulate the original dynamic trajectory optimization problem into a static nonlinear programming (NLP) problem. By doing so, the parameterized optimal trajectory, which has the maximum net power generation, can be obtained. To attenuate the strong nonlinear, multivariable and coupling characteristics of the flexible parafoil, a bandwidth parameterized linear extended state observer (ESO) is used to estimate and reject these dynamics explicitly in a unified way. Finally, the simulation results demonstrate the effectiveness of the proposed parameterized trajectory optimization and control strategies. The main contribution of this study is that complicated nonlinear parafoil dynamics with a complex trajectory can be well regulated by a PID-type linear time-invariant controller, which is appealing for practitioners.

Keywords: pseudospectral method (PSM); trajectory optimization; nonlinear programming (NLP); extended state observer (ESO)

Citation: Long, X.; Sun, M.; Piao, M.; Chen, Z. Parameterized Trajectory Optimization and Tracking Control of High Altitude Parafoil Generation. *Energies* **2021**, *14*, 7460. https://doi.org/10.3390/en14227460

Academic Editor: Luigi Costanzo

Received: 23 September 2021
Accepted: 3 November 2021
Published: 9 November 2021

1. Introduction

Wind power generation has a long history, and R&D in wind energy technology has never stopped [1,2]. However, traditional ground-based wind power generation has many shortcomings. Firstly, conventional wind power is mainly generated below 200 m [3], where the wind speed is low and turbulent. Secondly, site construction and equipment installation are complex and expensive, and the cost is proportional to the quintic power of the blade altitude [4]. Thirdly, a ground generator can only be located in areas with sufficient perennial wind; therefore, its deployment is limited. Compared with ground wind, wind at high altitudes has a high speed and a steady direction.

High altitude wind power generation (HAWPG) technology was gradually developed. Generally speaking, high altitudes are those higher than 200 m in the literature [5]. It is found that the wind energy density increases by 0.25–0.37 W/m^2 per meter in altitude [6]. When the altitude is 500 m, the average wind energy density is twice that of ground wind energy density. When altitude is 1000 m, wind energy density is about five times that of ground wind energy density. HAWPG can capture wind energy at high altitudes. The overall advantages of HAWPG are as follows: (1) a larger wind energy density at high altitudes; (2) lower land demand and construction costs; (3) mobile deployment and diversified application scenarios.

HAWPG is a new way to generate electricity, connecting the parafoil with the ground base station through one or two cables. The parafoil is manipulated at one end of the cable

to fly along a specific trajectory in order to drive the generator to produce electricity [7]. Wind energy can be collected at different altitudes, mainly dependent on the length of the cable. HAWPG has many advantages, however, there are still many technical problems to resolve, such as the parafoil trajectory optimization and control [8], which plays a crucial role in the economic benefit of this unique generator.

Firstly, the optimal trajectory of the parafoil at high altitudes has an unconventional shape with sufficiently high degrees of freedom, which have a great influence on power generation and should be designed carefully and concisely, such that the optimal trajectory can be conveniently programmed within the embedded microchip. Secondly, the parafoil at high altitudes has strong nonlinear, multivariable and coupling characteristics, which imposes a great challenge to accurate tracking. In practice, the parameterized design is appealing due to its simplification. In fact, the control computer for HAWPG is an embedded microchip, which has limited computational capability and memory space. Therefore, an efficient guidance and control algorithm with low computational complexity is urgently needed to meet the hardware requirements. Therefore, it is particularly important to seek a comprehensively parameterized trajectory optimization and path tracking control strategy for HAWPG, to facilitate its implementation.

In the past two decades, tentative investigations have been conducted on trajectory optimization and path tracking for HAWPG. Lord [9] derived an analytical formula for cable tension and analyzed the power generation of a kite with a circular motion. Zgraggen [10,11] investigated the sensitivity of the traction force to the path parameters and proposed a novel path optimization algorithm, wherein the characteristic parameters could be tuned using experimental data, in order to maximize power generation with limited wind information. Williams [12] optimized the trajectory of the parafoil for power generation and obtained the relationship between cable tension and the wind. Here, two cases were analyzed; one is the fixed rope length, the other is the varying rope length in a controlled manner within specified limits. The application of the nonlinear model predictive control (NMPC) method on parafoil trajectory optimization is quite appealing [13,14], due to its unique capability of dealing with multiple constraints within an optimization framework. However, an explicit solution cannot be obtained via NMPC, which is a prerequisite condition for programming the optimal trajectory in an embedded microchip. Therefore, the application of the NMPC on the parafoil remains unclear.

In recent years, many methods of trajectory optimization have emerged [15]. For example, the pseudospectral method (PSM) has been widely used in trajectory optimization [16,17]. In the PSM, the unknown state variables and control signals are parameterized on a series of Legendre–Gauss–Radau (LGR) points, and the Lagrange interpolation polynomials are used to approximate the real state variables and control signals. Then, the PSM can reformulate the original dynamic trajectory optimal problem into a static nonlinear programming (NLP) problem. Finally, the parameterized optimal trajectory can be obtained.

Elnagar [16] was the first to apply the PSM to optimal control, and he proved the feasibility of the transformation from an optimal control problem (OCP) to an NLP. The PSM has been applied well in trajectory optimization, such as in aircraft trajectory optimization [18], anti-swing trajectory planning [19], UAV formation trajectory optimization [20], and so on. Besides trajectory optimization, the path tracking control for HAWPG is also a great challenge. Erhard [21] proposed a cascade controller and demonstrated its effectiveness through flight tests. Fagiano [22] proposed a control method based on the wing velocity angle, which has few parameters to tune and does not require wind speed; this method was also demonstrated by experiments.

Li [23] designed a Lyapunov-based rotational nonlinear controller to achieve parafoil trajectory tracking. The control objective is to track a constant attack angle of the parafoil. Jiang and Hamid developed adaptive laws by taking advantage of the lower and upper bounded slowly varying time-delay information for the unknown nonlinearities [24]. These tracking strategies can be applied to the parafoil; however, the complexity of these

algorithms should be further reduced to match the microchip capacity and the dependence on the model dynamics should be weak to enhance robustness. This requires us to consider additional factors, other than the strong nonlinear and coupling characteristics, such as the remarkable uncertainties of the aerodynamics and external environment.

In practice, a model-free framework of the parafoil path tracking strategy is needed, which should be similar to the traditional proportional-integral-derivative (PID) controller because the practitioners are quite familiar with this. Han [25] proposed active disturbance rejection control (ADRC), which does not rely on a refined dynamic model. By making use of the linear gains, Gao [26] developed a concise linear ADRC which has fewer parameters and can be easily tuned in practice. Several breakthroughs for the control of nonlinear uncertain systems, made possible by ADRC, are discussed by Huang and Xue [27]. The essence of the ADRC is a linear extended state observer (ESO) which can extract the entire dynamic of the plant, with the exception of the control term as the total disturbance. According to the characteristics of the ESO, it is also expected to achieve satisfactory path tracking performance for the parafoil.

The main contribution of this paper is the path optimization and tracking of HAWPG in a comprehensively parameterized manner. The Radau PSM is used to obtain the optimal parafoil trajectory with the maximum net power generation and the trajectory can be realized with 41 LGR sampling points, which can meets the microchip requirement. Then, the parameterized ESO is used to estimate and reject the uncertain dynamics of the parafoil, such that accurate tracking can be achieved in the absence of precise model information in the control design.

The rest of this paper is organized as follows: the dynamic model of HAWPG is introduced in Section 2. Section 3 presents the parameterized trajectory optimization based on PSM. In Section 4, the parameterized ESO of the parafoil trajectory tracking control is provided. Section 5 provides the results of several simulations, including Monte Carlo tests. The concluding remarks are given in Section 6.

2. Parafoil Model and Problem Formulation

2.1. Model Establishment

The parafoil model nomenclature is given in Table 1.

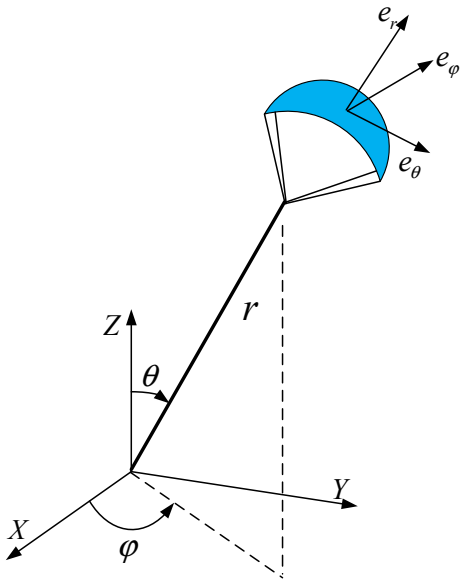

Figure 1. Parafoil in the ground coordinate system.

Table 1. Nomenclature.

θ	Spherical coordinate in Figure 1.	$[^\circ]$
φ	Spherical coordinate in Figure 1.	$[^\circ]$
r	Cable length in Figure 1.	[m]
$\dot{r}$	Cable changing rate	[m/s]
$\ddot{r}$	Cable acceleration	$[m/s^2]$
$\mathbf{e}_\theta$	Coordinate axis in Figure 1.	$[-]$
$\mathbf{e}_\varphi$	Coordinate axis in Figure 1.	$[-]$
$\mathbf{e}_r$	Coordinate axis in Figure 1.	$[-]$
$\mathbf{e}_0$	$= \mathbf{e}_r \times \mathbf{e}_\mathrm{w}$	$[-]$
$\mathbf{e}_\mathrm{w}$	$= \mathbf{W}_\mathrm{e}^\mathrm{p} / \left\lvert \mathbf{W}_\mathrm{e}^\mathrm{p} \right\rvert$	$[-]$
A	Parafoil area	$[m^2]$
A_c	Area of the line on the effective wind	$[m^2]$
m	Parafoil mass	[kg]
ρ	Air density	$[kg/m^3]$
ρ_c	Cable density	$[kg/m^3]$
d_c	Cable diameter	[m]
H	Parafoil actual height	[m]
H_ref	Reference altitude	[m]
W_ref	Reference wind velocity	[m/s]
C_L	Parafoil coefficient of lift	$[-]$
C_D	Parafoil coefficient of drag	$[-]$
$C_\mathrm{c,D}$	Cable coefficient of drag	$[-]$
E	$= C_\mathrm{L}/C_\mathrm{D}$	$[-]$
Δl	Cable length difference at the two ends of the traction parafoil in Figure 2.	[m]
d	Length of the wingspan in Figure 2.	[m]
ψ	$= \arcsin(\Delta l/d)$ in Figure 2.	$[^\circ]$
$\Delta\alpha$	Angle between the effective wind velocity and the (e_θ, e_φ) plane	$[^\circ]$
$\mathbf{W}_\mathrm{e}$	Effective wind speed	[m/s]
$\mathbf{W}_\mathrm{e}^\mathrm{p}$	Projection and unit vector of the effective wind speed on the (e_θ, e_φ) plane	[m/s]
$\mathbf{X}_\mathrm{w}$	Wind coordinate axis	$[-]$
$\mathbf{Y}_\mathrm{w}$	Wind coordinate axis	$[-]$
$\mathbf{Z}_\mathrm{w}$	Wind coordinate axis	$[-]$
F^grav	Parafoil and cable weight	[N]
F^aer	Parafoil aerodynamic force	[N]
$F^\mathrm{c,aer}$	Cable aerodynamic force	[N]
F^app	Apparent force	[N]
$F^\mathrm{c,trc}$	Cable traction force	[N]
$F_\mathrm{L}^\mathrm{aer}$	Aerodynamic lift force	[N]
$F_\mathrm{D}^\mathrm{aer}$	Aerodynamic drag force	[N]

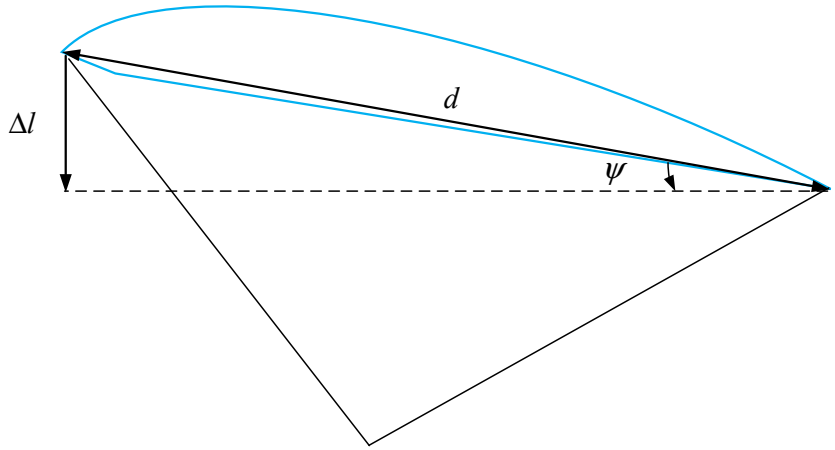

Figure 2. Roll angle ψ.

The kinematic model of the parafoil is established as shown in Figure 1. In the ground coordinate system, the angle between the cable and the Z axis is θ, the angle between the projection of the cable on the XY plane and the X axis is φ, and the length of the cable is r, then the parafoil velocity $\dot{\mathbf{P}}$ in the coordinate system is:

$$\dot{\mathbf{P}} = \begin{pmatrix} \dot{\theta} r \\ \dot{\varphi} r \sin\theta \\ \dot{r} \end{pmatrix} \tag{1}$$

The spherical coordinate system is introduced to facilitate the force analysis of the parafoil. The transformation from the ground coordinate system to the spherical coordinate system is:

$$\begin{pmatrix} \mathbf{e}_\theta & \mathbf{e}_\varphi & \mathbf{e}_r \end{pmatrix} = \begin{pmatrix} \cos\theta\cos\varphi & -\sin\varphi & \sin\theta\cos\varphi \\ \cos\theta\sin\varphi & \cos\varphi & \sin\theta\sin\varphi \\ -\sin\theta & 0 & \cos\theta \end{pmatrix} \tag{2}$$

The aerodynamic force of the parafoil is mainly related to the relative speed and direction of the wind; therefore, it is necessary to establish the wind coordinate system. The wind speed W_h can be approximated as:

$$\begin{cases} W_\mathrm{h} = -W_\mathrm{ref}\left(\frac{H}{H_\mathrm{ref}}\right)^n \\ H = r\cos\theta \end{cases} \tag{3}$$

where $n = 1/7$ is given by ITTC [28]. To calculate the parafoil aerodynamic force, the effective wind speed is used. To simplify the calculation, we assume that the wind direction is in the negative direction of the X axis. The effective wind speed is:

$$\mathbf{W}_\mathrm{e} = W_\mathrm{h} - \dot{\mathbf{P}} \tag{4}$$

The projection and the unit vector of the effective wind speed on the (e_θ, e_φ) plane is:

$$\mathbf{W}_\mathrm{e}^\mathrm{p} = \begin{pmatrix} 1 & 0 & 0 \\ 0 & 1 & 0 \\ 0 & 0 & 0 \end{pmatrix} \mathbf{W}_\mathrm{e} \tag{5}$$

and

$$\mathbf{e}_\mathrm{w} = \frac{\mathbf{W}_\mathrm{e}^\mathrm{p}}{\left|\mathbf{W}_\mathrm{e}^\mathrm{p}\right|} \tag{6}$$

respectively. The parafoil wind coordinate is:

$$\begin{cases} \mathbf{X}_{\mathrm{w}} = -\frac{\mathbf{W}_{\mathrm{e}}}{|\mathbf{W}_{\mathrm{e}}|} \\ \mathbf{Y}_{\mathrm{w}} = -\mathbf{e}_{\mathrm{w}}\left(\frac{\mathbf{e}_r \cdot \mathbf{W}_{\mathrm{e}}}{|\mathbf{W}_{\mathrm{e}}^{\mathrm{p}}|}\right)\sin\psi + \mathbf{e}_0 + \mathbf{e}_r \sin\psi \\ \mathbf{Z}_{\mathrm{w}} = \mathbf{X}_{\mathrm{w}} \times \mathbf{Y}_{\mathrm{w}} \end{cases} \tag{7}$$

The traction parafoil is inflated as shown in Figure 2.

The forces acting on the parafoil can be projected in three directions: e_θ, e_φ and e_r. Each such projection can be further decomposed into four parts according to its originality, that is the cable and parafoil gravity F^{grav}, the aerodynamic force F^{aer}, the cable aerodynamic resistance $F^{\mathrm{c,aer}}$, and the apparent forces F^{app}. In addition, there is cable traction $F^{\mathrm{c,trc}}$. In the spherical coordinate system, these terms can be written as:

$$\begin{cases} F_\theta = F_\theta^{\mathrm{grav}} + F_\theta^{\mathrm{aer}} + F_\theta^{\mathrm{c,aer}} + F_\theta^{\mathrm{app}} \\ F_\varphi = F_\varphi^{\mathrm{grav}} + F_\varphi^{\mathrm{aer}} + F_\varphi^{\mathrm{c,aer}} + F_\varphi^{\mathrm{app}} \\ F_r = F_r^{\mathrm{grav}} + F_r^{\mathrm{aer}} + F_r^{\mathrm{c,aer}} + F_r^{\mathrm{app}} - F^{\mathrm{c,trc}} \end{cases} \tag{8}$$

1. The parafoil and the cable gravity is:

$$\mathbf{F}^{\mathrm{grav}} = \begin{pmatrix} F_\theta^{\mathrm{grav}} \\ F_\varphi^{\mathrm{grav}} \\ F_r^{\mathrm{grav}} \end{pmatrix} = \begin{pmatrix} \left(m + \frac{\rho_{\mathrm{c}}\pi d_{\mathrm{c}}^2 r}{4}\right) g\sin\theta \\ 0 \\ -\left(m + \frac{\rho_{\mathrm{c}}\pi d_{\mathrm{c}}^2 r}{4}\right) g\cos\theta \end{pmatrix} \tag{9}$$

2. The parafoil aerodynamic force (the forces acting on the parafoil in motion relative to the air, which includes aerodynamic lift $F_{\mathrm{L}}^{\mathrm{aer}}$ and aerodynamic drag $F_{\mathrm{D}}^{\mathrm{aer}}$ is:

$$\mathbf{F}^{\mathrm{aer}} = \begin{pmatrix} F_\theta^{\mathrm{aer}} \\ F_\varphi^{\mathrm{aer}} \\ F_r^{\mathrm{aer}} \end{pmatrix} = -\frac{1}{2}C_{\mathrm{D}}A\rho|\mathbf{W}_{\mathrm{e}}|^2\mathbf{X}_{\mathrm{w}} - \frac{1}{2}C_{\mathrm{L}}A\rho|\mathbf{W}_{\mathrm{e}}|^2(\mathbf{X}_{\mathrm{w}} \times \mathbf{Y}_{\mathrm{w}}) \tag{10}$$

3. The cable aerodynamic resistance is:

$$\mathbf{F}^{\mathrm{c,aer}} = \begin{pmatrix} F_\theta^{\mathrm{c,aer}} \\ F_\varphi^{\mathrm{c,aer}} \\ F_r^{\mathrm{c,aer}} \end{pmatrix} = -\frac{1}{8}\rho C_{\mathrm{c,D}}A_{\mathrm{c}}\cos(\Delta\alpha)|\mathbf{W}_{\mathrm{e}}|^2\mathbf{X}_{\mathrm{w}} \tag{11}$$

$\Delta\alpha$ is the angle between the effective wind velocity $\mathbf{W}_{\mathrm{e}}$ and the (e_θ, e_φ) plane (in Figure 3) as:

$$\Delta\alpha = \arcsin\left(\frac{\mathbf{e}_r \cdot \mathbf{W}_{\mathrm{e}}}{|\mathbf{W}_{\mathrm{e}}|}\right) \tag{12}$$

4. Apparent forces.

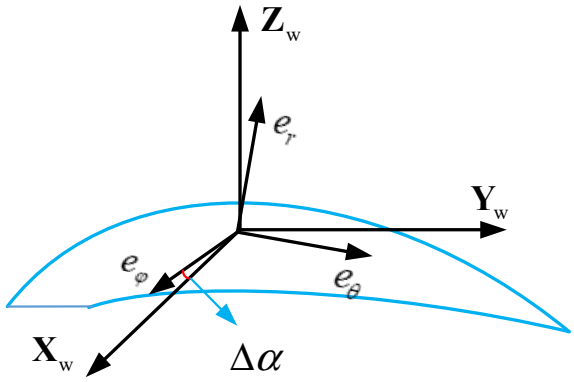

Figure 3. Definition of $\Delta\alpha$.

In addition, the particular force dependent on the considered parafoil generator configuration should also be included. For example, the apparent force defined as the centrifugal inertial force is represented as:

$$\mathbf{F}^{\text{app}} = \begin{pmatrix} F_{\theta}^{\text{app}} \\ F_{\varphi}^{\text{app}} \\ F_{r}^{\text{app}} \end{pmatrix} = \begin{pmatrix} m(\dot{\varphi}^2 r \sin\theta\cos\theta - 2\dot{r}\dot{\theta}) \\ m(-2\dot{r}\dot{\varphi}\sin\theta - 2\dot{\varphi}\dot{\theta}r\cos\theta) \\ m(\dot{r\theta}^2 + r\dot{\varphi}^2\sin^2\theta) \end{pmatrix} \tag{13}$$

5. The cable traction force is shown in Figure 4:

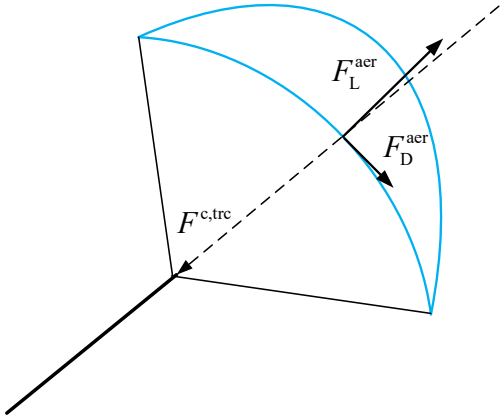

Figure 4. Aerodynamic forces $F_{\text{L}}^{\text{aer}}$ and $F_{\text{D}}^{\text{aer}}$, cable traction $F^{\text{c,trc}}$ on a parafoil.

According to Figure 4, the aerodynamic lift force, $F_{\text{L}}^{\text{aer}}$, the aerodynamic drag force,$F_{\text{D}}^{\text{aer}}$, and the cable traction, $F^{\text{c,trc}}$, satisfy the Pythagorean theorem. Therefore, the cable traction can be derived from the aerodynamic lift and drag forces as:

$$F^{\text{c,trc}} = \sqrt{\left(F_{\text{L}}^{\text{aer}}\right)^2 + \left(F_{\text{D}}^{\text{aer}}\right)^2} \tag{14}$$

Combining (14) with Equation (10) yields:

$$\begin{aligned} F^{\text{c,trc}} &= -\left(-\tfrac{1}{2}\rho A|\mathbf{W}_{\text{e}}|^2\sqrt{{C_{\text{L}}}^2 + {C_{\text{D}}}^2}\right) \\ &= \tfrac{1}{2}\rho A|\mathbf{W}_{\text{e}}|^2 C_{\text{L}}\sqrt{1 + \left(\tfrac{C_{\text{D}}}{C_{\text{L}}}\right)^2} \\ &= \tfrac{1}{2}\rho A|\mathbf{W}_{\text{e}}|^2 C_{\text{L}}\sqrt{\left(\tfrac{E^2+1}{E^2}\right)} \end{aligned} \tag{15}$$

where $E = C_{\text{L}}/C_{\text{D}}$ is the lift-drag ratio.

There are eight state variables and three control signals in the parafoil model, expressed as:

$$x = [x_1, x_2, x_3, x_4, x_5, x_6, x_7, x_8]^T = [\theta, \varphi, r, \dot{\theta}, \dot{\varphi}, \dot{r}, C_L, \psi]^T$$

and,

$$u = [u_1, u_2, u_3]^T = \left[\ddot{r}, \dot{C}_L, \dot{\psi}\right]^T.$$

In summary, the parafoil model can be written as:

$$\dot{x}(t) = \begin{bmatrix} \dot{\theta} \\ \dot{\varphi} \\ \dot{r} \\ \frac{F_\theta}{mr} \\ \frac{F_\varphi}{mr\sin\theta} \\ \frac{F_r}{m} \\ \dot{C}_L \\ \dot{\psi} \end{bmatrix} \tag{16}$$

2.2. Problem Formulation

The objective of the trajectory optimization for HAWPG is to obtain the maximum power generation. The parafoil power generation is just the multiplication of the cable changing rate $\dot{r}$ and the cable tension $F^{c,trc}$ as:

$$P = \dot{r}F^{c,trc} \tag{17}$$

In a period of T, the generation power can be given as:

$$W(T) = \int_0^T P(t)dt \tag{18}$$

The average power is usually used to measure the amount of power, which can be written as:

$$\begin{aligned} \overline{P} &= \frac{W(T)}{T} \\ &= \frac{1}{T}\int_0^T P(t)dt \\ &= \frac{1}{T}\int_0^T \dot{r}(t)F^{c,trc}(t)dt \end{aligned} \tag{19}$$

The cost function to be minimized is:

$$J = -\frac{1}{T}\int_0^T \dot{r}(\tau)F^{c,trc}(\tau)d\tau \tag{20}$$

2.3. OCP Formulation

The optimization problem of HAWPG is described as:

$$\min \quad J$$
$$s.t. \begin{cases} \forall t \in [0,T] : \dot{x}(t) = f(x(t), u(t), t) \\ \forall t \in [0,T] : g(x(t), u(t), t) \le 0 \\ \forall t \in [0,T] : r(x(0), x(T)) = 0 \end{cases} \tag{21}$$

where,

$$f(x(t),u(t),t)=\begin{bmatrix}\dot{x}_1\\ \dot{x}_2\\ \dot{x}_3\\ \dot{x}_4\\ \dot{x}_5\\ \dot{x}_6\\ \dot{x}_7\\ \dot{x}_8\end{bmatrix}=\begin{bmatrix}x_4\\ x_5\\ x_6\\ \frac{F_\theta}{mr}\\ \frac{F_\varphi}{mr\sin\theta}\\ u_1\\ u_2\\ u_3\end{bmatrix} \tag{22}$$

Additionally $g(x(t),u(t),t)$ is an inequality constraint, including $x_{\min}\le x\le x_{\max}$, and $u_{\min}\le u\le u_{\max}$. $r(x(0),x(T))$ is the boundary condition which ensures that the whole power generation process is repetitive, which satisfies $x(0)=x(T)$.

3. Parameterized Trajectory Optimization

In this section, the PSM is used to optimize the trajectory. The unknown state variables and control signals are parameterized in a series of LGR points, and the Lagrange interpolation polynomials are used to approximate the real state variables and control signals. Then, the PSM can be reformulated from the original dynamic optimal trajectory problem into a static NLP problem. Finally, the parameterized optimal trajectory can be obtained. The PSM can be divided into the following four parts:

1. Time domain conversion:

For HAWPG, the initial time is $t_0=0$ and the terminal time is $t_\mathrm{f}=T$, in a given period. The $t\in[0,T]$ in the original problem can be mapped onto the time interval $[-1,1]$ as:

$$\tau=\frac{2t}{T-0}-\frac{T+0}{T-0} \tag{23}$$

where $\tau\in[-1,1]$. At this time interval, the above problems can be transformed into a standard Bolza problem as:

$$\begin{aligned}\min\quad & J=\Phi(x(-1),x(1),0,T)+\tfrac{T-0}{2}\textstyle\int_{-1}^{1}L(x(\tau),u(\tau),\tau)d\tau\\ s.t.\begin{cases}\frac{dx}{d\tau}=\frac{T-0}{2}f(x(\tau),u(\tau),\tau;0,T)\\ x_{\min}\le x\le x_{\max},u_{\min}\le u\le u_{\max}\\ x(0)=x(T)\end{cases}\end{aligned} \tag{24}$$

2. Calculation of the distribution nodes:

The LGR point is the zero of the $P_{N-1}(\tau)+P_N(\tau)$, where $P_N(\tau)$ is the Legendre polynomial order N as:

$$P_N(\tau)=\frac{1}{2^N N!}\frac{d^N}{d\tau^N}\left[(\tau^2-1)^N\right] \tag{25}$$

There are $N-1$ such points that are in the interval $[-1,1]$, and the endpoint -1 is also such a point.

3. State and control variables parameterization:

The state variables x_i and the control signals u_i are the values at the LGR points τ_i, $i=1,2,\ldots,N$. The Lagrange interpolation polynomials are used to approximate the state and control curves as:

$$\begin{aligned}x(\tau)\quad&\approx X(\tau)=\sum_{i=1}^{N}L_i(\tau)X(\tau_i)\\ &=\sum_{i=1}^{N}L_i(\tau)X_i\end{aligned} \tag{26}$$

and

$$\begin{aligned} u(\tau) &\approx U(\tau) = \sum_{i=1}^{N} L_i(\tau) U(\tau_i) \\ &= \sum_{i=1}^{N} L_i(\tau) U_i \end{aligned} \tag{27}$$

where $L_i(\tau)$ is the Lagrange interpolation base function:

$$L_i(\tau) = \prod_{j=1, j\neq i}^{N} \frac{\tau - \tau_j}{\tau_i - \tau_j} \tag{28}$$

4. Elimination of the dynamic equations.

In the above-mentioned optimal control problem, the state equations have derivative forms, while the cost function is in the integral form with respect to the time variables, respectively. However, we must resort to the static optimizer to solve this dynamic problem. Therefore, a reformulation should be conducted by using the LGR nodes. The derivative operation can be eliminated according to the following steps:

$$\dot{x}(\tau) \approx \dot{X}(\tau) = \sum_{i=1}^{N} \dot{L}_i(\tau) X_i = \sum_{i=1}^{N} D_{k,i} X_i \tag{29}$$

and

$$\sum_{i=1}^{N} D_{k,i} X_i = \frac{T-0}{2} f(X_k, U_k, \tau_k; 0, T) \tag{30}$$

where D is the matrix with dimension $(N-1) \times N$, which is called the state differential matrix. The integral operation can be approximated as

$$\begin{aligned} &\int_{\sum 1}^{1} L(x(\tau), u(\tau), \tau; 0, T) \\ &\approx \sum_{k=1}^{N-1} \omega_k L(x(\tau), u(\tau), \tau; 0, T) \\ &= \sum_{k=1}^{N-1} \omega_k L(X_k, U_k, \tau_k; 0, T) \end{aligned} \tag{31}$$

where $\omega_k = \int_{-1}^{1} L_i(\tau) d\tau$, is the integral weight.

Through the above steps, the original problem can be reformulated into a static NLP as:

$$\begin{aligned} \min \quad & J = \Phi(X_0, 0, X_N, T) + \tfrac{T-0}{2} \sum_{k=1}^{N-1} \omega_k L(X_k, U_k, \tau_k; 0, T) \\ s.t. & \begin{cases} \sum_{i=1}^{N} D_{k,i} X_i = \tfrac{T-0}{2} f(X_k, U_k, \tau_k; 0, T) \\ X_{\min} \leq X_k \leq X_{\max}, U_{\min} \leq U_k \leq U_{\max} \\ X(0) = X(T) \end{cases} \end{aligned} \tag{32}$$

Then, the problem can be solved directly by using the optimizer of the PSM. Therefore, the parameterized optimal trajectory of the parafoil under multiple constraints can be obtained.

4. Trajectory Tracking Control

When the optimal trajectory of HAWPG is obtained, the next step is to design an effective tracking method to realize it. Here, a linear controller is proposed and a parameterized observer is used to estimate and compensate these complicated dynamics explicitly.

The kinematic model of the parafoil is:

$$\begin{cases} \ddot{\theta} = \frac{F_\theta}{mr} \\ \ddot{\varphi} = \frac{F_\varphi}{mr\sin\theta} \end{cases} \tag{33}$$

In the trajectory tracking design, the pitch and yaw angles are selected as the regulated outputs. The parafoil dynamics can be regarded as second-order nonlinear plants, which have the forms of

$$\begin{cases} \ddot{\theta} = f_1(\cdot) + b_1(t)u_1(t) + b_4(t)u_2(t) \\ \ddot{\varphi} = f_2(\cdot) + b_2(t)u_2(t) + b_3(t)u_1(t) \end{cases} \tag{34}$$

where $f_1(\cdot)$ and $f_2(\cdot)$ are the combined nonlinear dynamics, $b_i(t), (i = 1, \ldots, 4)$ are the control gains, $u_1(t)$ is the lift coefficient, and $u_2(t)$ is the roll angle, respectively. By defining $x_{11} = \theta$, $x_{12} = \dot{\theta}$, $x_{21} = \varphi$, $x_{22} = \dot{\varphi}$, Equation (36) can be represented as:

$$\begin{cases} \dot{x}_{11} = x_{12} \\ \dot{x}_{12} = x_{13} + b_1 u_1 \\ \dot{x}_{13} = f_1 \\ y_1 = x_{11} \end{cases} \tag{35}$$

$$\begin{cases} \dot{x}_{21} = x_{22} \\ \dot{x}_{22} = x_{23} + b_{02} u_2 \\ \dot{x}_{23} = f_2 \\ y_2 = x_{21} \end{cases} \tag{36}$$

where f_1 and f_2 contain the major dynamic uncertainties, which should be attenuated to enhance robustness. It should be noted that f_1 and f_2 have no explicit physical meanings, and they are just the remaining parts, except for the direct control terms. These variable states x_{13} and x_{23} are defined as extended states [25] because they are not the original states of the dynamics. A straightforward philosophy would be to reject it, such that integrator chains can be achieved to employ mature linear controllers. However, these states cannot be measured or calculated directly. Therefore, an appropriate estimation is necessary. To obtain the estimation of this state, two observers can be designated as:

$$\begin{cases} e_1 = z_{11} - \theta \\ \dot{z}_{11} = z_{12} - 3\omega_{o1} e_1 \\ \dot{z}_{12} = z_{13} - 3\omega_{o1}^2 e_1 + b_{01} u_1 \\ \dot{z}_{13} = -\omega_{o1}^3 e_1 \end{cases} \tag{37}$$

$$\begin{cases} e_2 = z_{21} - \varphi \\ \dot{z}_{21} = z_{22} - 3\omega_{o2} e_2 \\ \dot{z}_{22} = z_{23} - 3\omega_{o2}^2 e_2 + b_{02} u_2 \\ \dot{z}_{23} = -\omega_{o2}^3 e_2 \end{cases} \tag{38}$$

where $[z_{11}, z_{12}, z_{13}]^T$ are the estimations for $[x_{11}, x_{12}, x_{13}]^T$. Similarly, $[z_{21}, z_{22}, z_{23}]^T$ are the estimations for $[x_{21}, x_{22}, x_{23}]^T$. Because the extended states are estimated through these observers, they are called the extended state observers (ESO) [25]. Here, ω_{o1} and ω_{o2} are the observer bandwidths. The controllers can then be designated as:

$$\begin{cases} u_1 = \frac{u_{01} - z_{13}}{b_{01}} \\ u_2 = \frac{u_{02} - z_{23}}{b_{02}} \end{cases} \tag{39}$$

where u_{01} and u_{02} are the control variables. Hence, the original plant can be reformulated as:

$$\begin{cases} \ddot{\theta} = u_{01} \\ \ddot{\varphi} = u_{02} \end{cases} \tag{40}$$

Because the regulated variables are the pitch and yaw angles, we can design two proportional-derivative (PD) controllers for u_{01} and u_{02} as:

$$\begin{cases} u_{01} = k_{p1}(\theta_r - z_{11}) - k_{d1}\left(\dot{\theta}_r - z_{12}\right) \\ u_{02} = k_{p2}(\varphi_r - z_{21}) - k_{d2}\left(\dot{\varphi}_r - z_{22}\right) \end{cases} \tag{41}$$

where θ_r and φ_r are the references for the pitch and yaw angles, respectively, k_{p1}, k_{d1}, k_{p2}, k_{d2} are the controller parameters and $\left[k_{p1}, k_{d1}\right] = \left[\omega_{c1}^2, 2\omega_{c1}\right]$, $\left[k_{p2}, k_{d2}\right] = \left[\omega_{c2}^2, 2\omega_{c2}\right]$, where ω_{c1} and ω_{c2} are the controller bandwidths. In summary, the control law for the pitch and yaw angles becomes:

$$\begin{cases} u_1 = \frac{k_{p1}(\theta_r - z_{11}) - k_{d1}\left(\dot{\theta}_r - z_{12}\right) - z_{13}}{b_{01}} \\ u_2 = \frac{k_{p2}(\varphi_r - z_{21}) - k_{d2}\left(\dot{\varphi}_r - z_{22}\right) - z_{23}}{b_{02}} \end{cases} \tag{42}$$

These controllers are based on ESO and are completely linear; thus, they are called linear active disturbance rejection controllers (LADRC) [26]. The entire control configuration is shown in Figure 5. The dynamics of the parafoil demonstrate strong nonlinearity. Traditionally, a complicated nonlinear controller is needed for this case. Here, LADRC is a linear control but its design concept is totally different from that of classical linear controllers and it can be applied to nonlinear, time-varying, and uncertain processes with very little model information. This is because the conventional linear controllers are generally based on a linearized model of nonlinear dynamics and they are model-based. By contrast, LADRC can be derived straightforwardly from nonlinear dynamics, and it treats nonlinear dynamics as a signal rather than a model. Then, there is no difference between linear and nonlinear dynamics when using ESO. Therefore, we can extend the application range of the linear controller to a wider kind of nonlinear dynamics. This is quite appealing for practitioners.

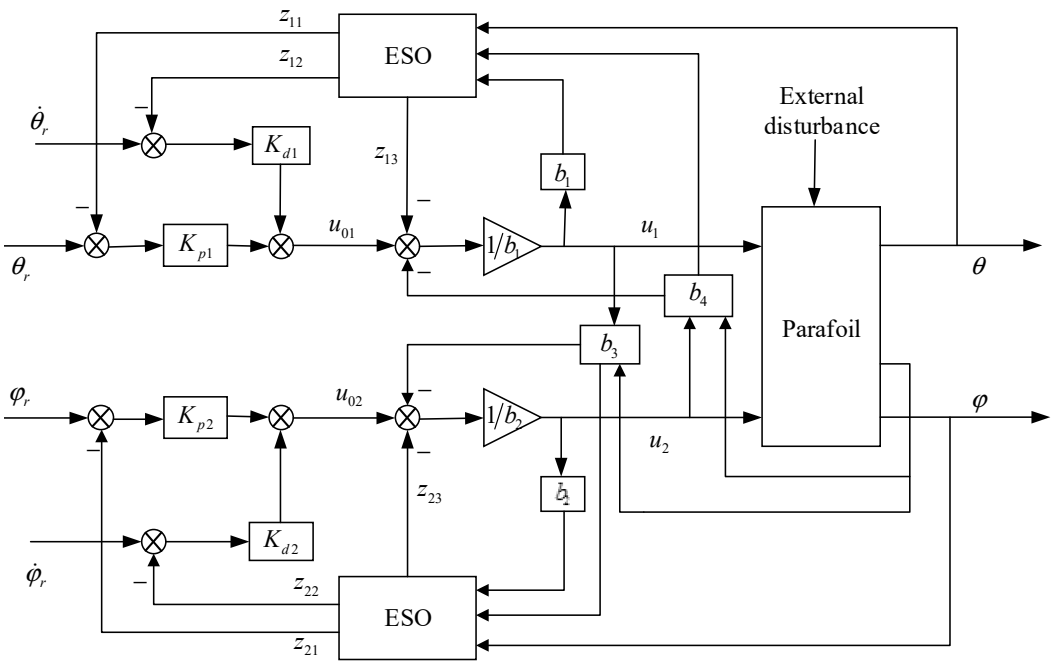

Figure 5. Block diagram of the double close-loop decoupled controller.

5. Optimization and Simulation Results

In this section, the effectiveness of the proposed method will be validated through a numerical example. The computer configuration is: Windows 10, 64-bit; Intel (R) Core (TM) i7-9750H CPU; the dominant frequency is 2.60 GHz; memory space is 16 GB; and, Matlab 2020b is used for the simulation. The characteristic parameters of the parafoil are shown in Table 2, while the state and control constraints are shown in Table 3.

Table 2. Parafoil model parameters.

m	850	Kite mass [kg]
A	500	Characteristic area $[m^2]$
ρ	1.23	Air density $[kg/m^3]$
ρ_c	970	Line density $[kg/m^3]$
d_c	0.056	Line diameter [m]
$C_{c,D}$	1	Line drag coefficient
H_{ref}	100	Reference altitude [m]
W_{ref}	10	Reference wind velocity [m/s]
g	9.81	Gravity acceleration $[m/s^2]$

Table 3. Constraints of the states and controls in the trajectory tracking by PSM.

Constraint Condition	Constraints	Range of the Constraints
State constraints	θ	$[25, 80]$
	φ	$[-30, 30]$
	r	$[1428, 1500]$
	ψ	$[-16, 16]$
	$\dot{\theta}$	$[-3, 3]$
	$\dot{\varphi}$	$[-1, 1]$
	$\dot{r}$	$[-15, 15]$
	C_L	$[0.1, 1.5]$
Control constraints	$\ddot{r}$	$[-25, 25]$
	$\dot{C}_L$	$[-2, 2]$
	$\dot{\psi}$	$[-1, 1]$

5.1. Optimization Results

The optimization objective is specified as the maximization of the net power generation in an operation cycle, as shown in Equation (20). We specify the generation period as $T = 20$ s. The parameterized optimal trajectory can be obtained by using the Gauss pseudospectral optimization software (GPOPS), and the optimized trajectory can be realized with 41 LGR sampling points. The optimal values for the states and controls at the specified LGR sampling points can be illustrated in Figures 6 and 7. The complete control and state curves can then be established using the Lagrange interpolation of Equations (28) and (29) directly according to these collocation points.

The optimal trajectory of a period is shown in Figure 8. As can be seen from Figure 8a, the optimal parafoil trajectory is approximately a figure eight. The three trajectory coordinates are shown in Figure 8b with smooth changes, which is convenient for subsequent path tracking. The eight states are shown in Figure 9a–h, respectively. The three control signals are shown in Figure 10. The boundary condition ensures that the whole power generation process is repetitive. The initial and terminal values of the lift should be equal, $C_L(0) = C_L(T)$. The power maximization attempts to achieve maximum cable traction by changing the lift coefficient in the early stage of optimization. Therefore, there will be spontaneous changes in the lift coefficient.

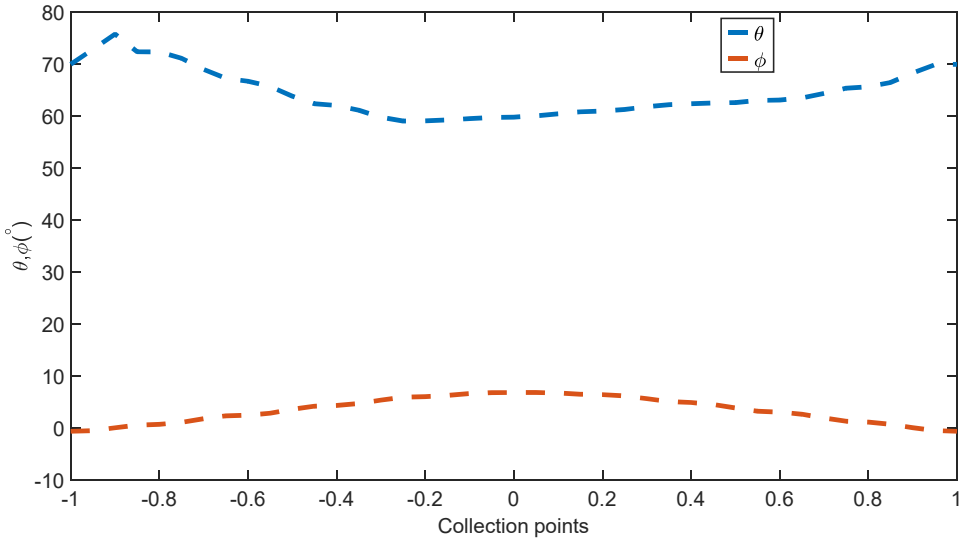

Figure 6. The LGR collection points of state variables (taking pitch and yaw angle as examples).

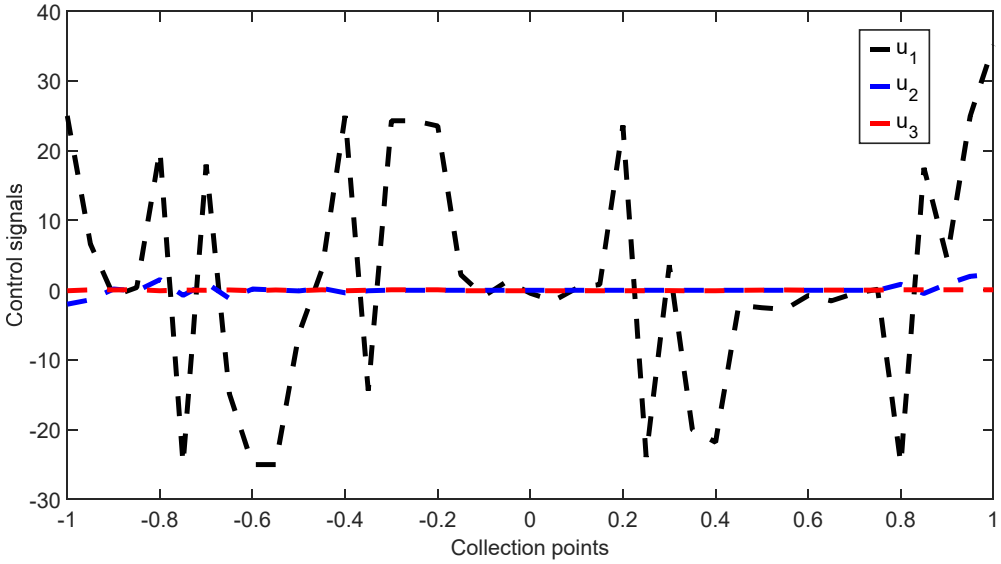

Figure 7. The LGR collection points of control signals.

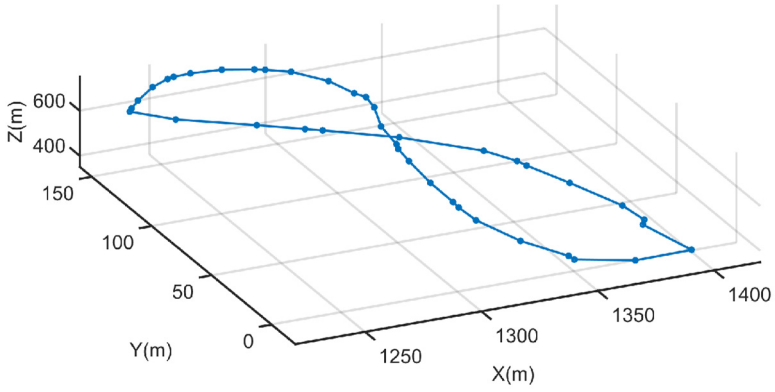

(**a**)

Figure 8. *Cont*.

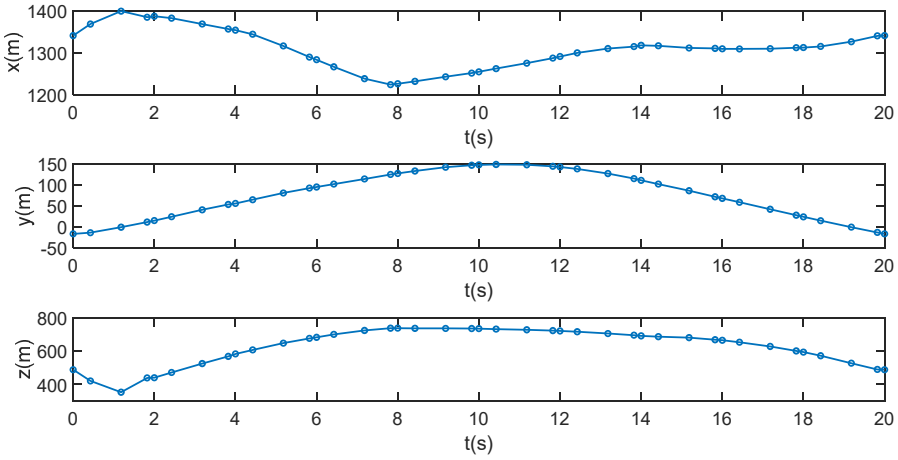

(**b**)

Figure 8. Optimal trajectory of the parafoil by PSM. (**a**) Three-dimensional trajectory; (**b**) Trajectory coordinates.

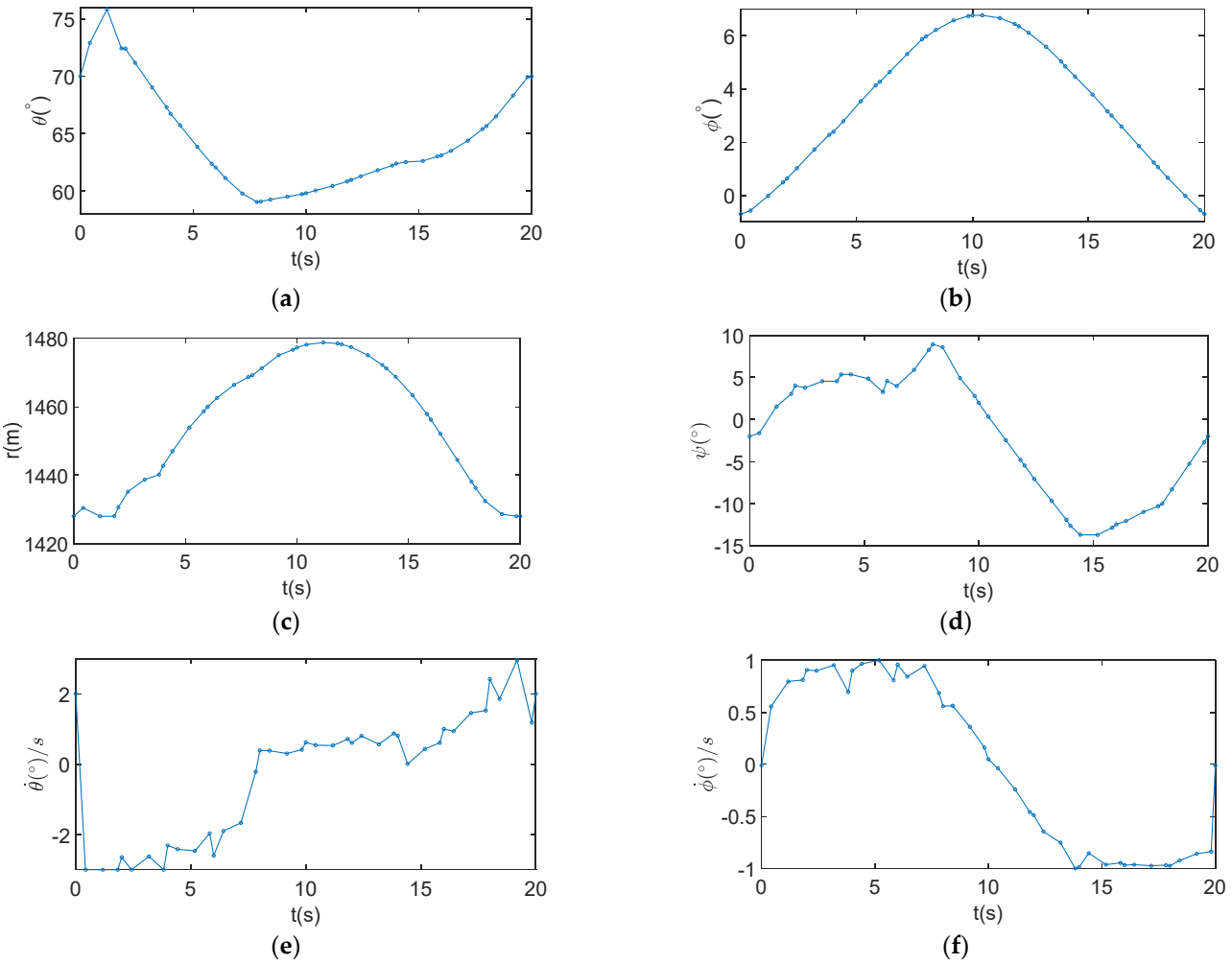

Figure 9. *Cont.*

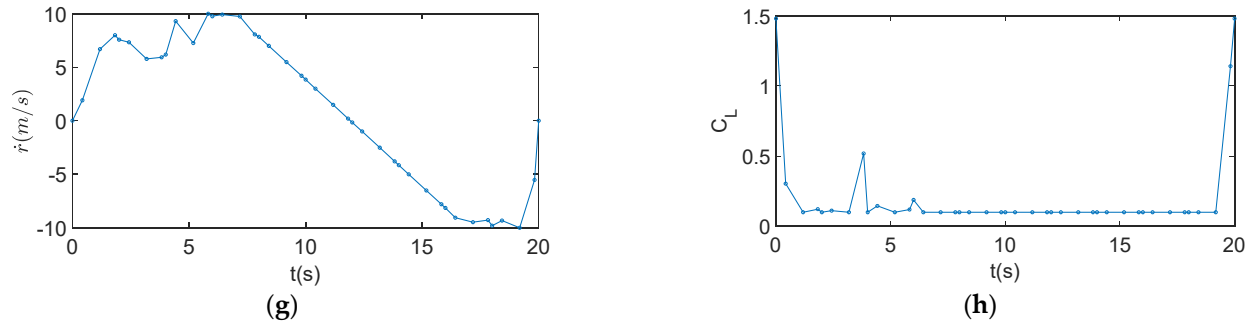

Figure 9. State variables' optimization results by PSM. (**a**) Pitch angle. (**b**) Yaw angle. (**c**) Cable length. (**d**) Roll angle. (**e**) Pitch angular rate. (**f**) Yaw angular rate. (**g**) Cable velocity. (**h**) Lift coefficient.

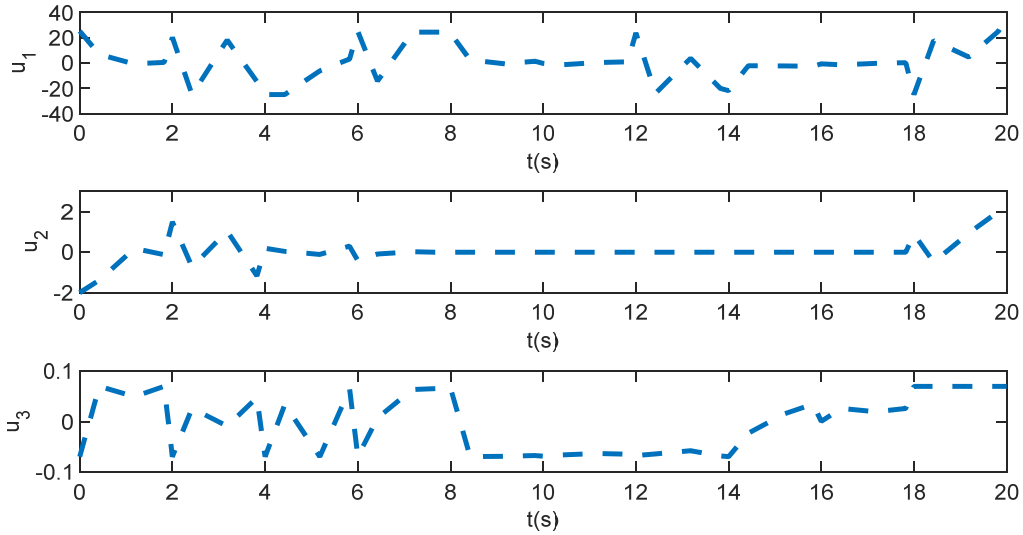

Figure 10. Control signals' optimization results by PSM. u_1 is the cable acceleration $\ddot{r}$, u_2 is the aerodynamic coefficient rate of change $\dot{C}_L$, u_3 is the roll angle rate $\dot{\psi}$.

Through the optimization solution, the cable traction force and the power generation can be seen from Figures 11 and 12. According to Figure 12, the parafoil is at the production stage before 12 s, then, the cable is pulled back at the energy consumption stage. Electricity generation is significantly greater than energy consumption in this period. Thus, the parafoil can obtain a considerable amount of electricity by repeating this movement at high altitudes.

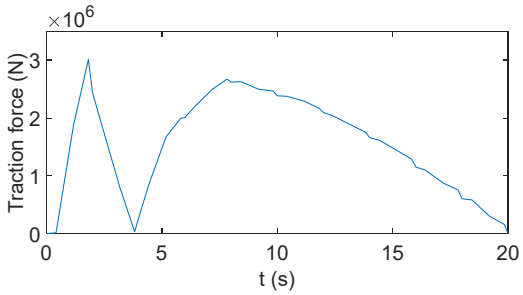

Figure 11. The change of cable traction force in trajectory optimization.

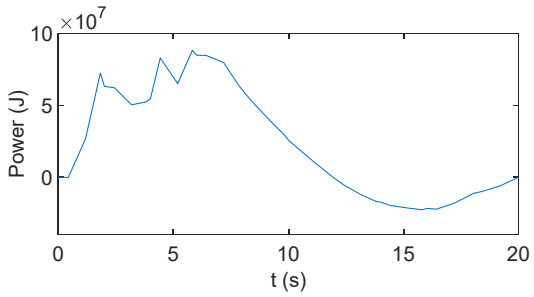

Figure 12. Power generation during the production and consumption stages.

5.2. Tracking Control Results

According to the above-mentioned results, the pitch and yaw angles obtained during optimization are specified as control commands. The control parameters are tuned as shown in Table 4.

Table 4. Control parameters of the pitch and yaw angle channels.

Control Parameters	Pitch Angle Channel	Yaw Angle Channel
ω_o	4	10
K_P	15	12
K_d	2.9	9
b	−11	13

The simulation results are shown in Figures 13–15. According to Figures 14 and 15, the optimal trajectory can be tracked efficiently with sufficient accuracy. This can demonstrate that the parameterized observer can estimate and reject the complicated nonlinear dynamics effectively.

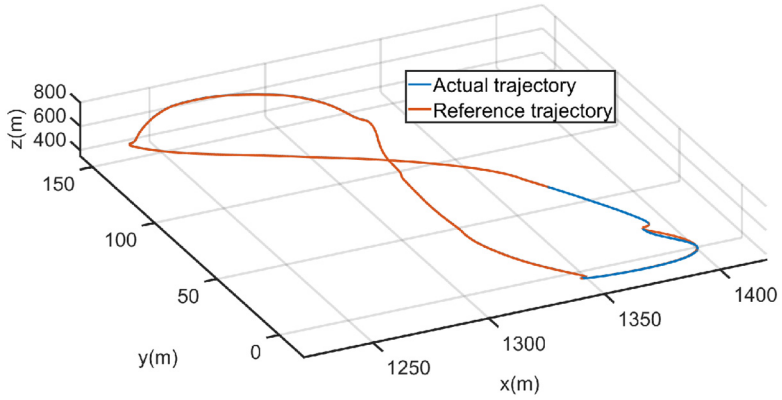

Figure 13. Three-dimensional tracking trajectory.

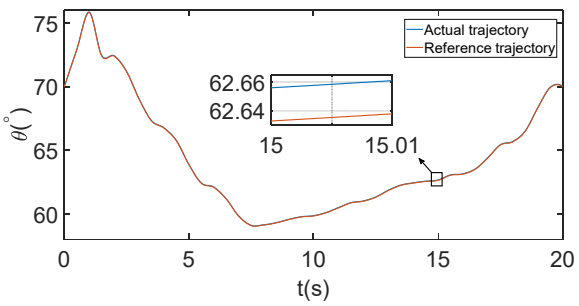

Figure 14. Pitch angle tracking result by LADRC controller.

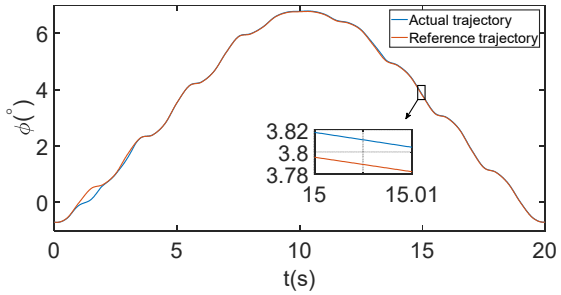

Figure 15. Yaw angle tracking result by LADRC controller.

5.3. Perturbed Cases and Monte Carlo Simulation

The uncertainties are considered to evaluate the robustness of the proposed method. In HAWPG, the uncertainties in the aerodynamic coefficients are the most important factors. There are three uncertain coefficients: C_L, C_D and $C_{c,D}$. In practice, 10% is the traditionally used uncertain range of the aerodynamic forces. We evaluate the robustness with perturbations shown in Table 5, and Table 6 shows the variation of the power generation outputs in a Monte Carlo simulation.

Table 5. Uncertain coefficients in Monte Carlo simulation.

C_L	C_D	$C_{c,D}$
±10%	±10%	±10%

Table 6. Generation power in Monte Carlo simulation.

Parametric Perturbation (%)	Generation Power ($\times 10^7$J)	Power Variation Rate (%)
C_L : 0 C_D : 0 $C_{c,D}$: 0	8.82	0.00
C_L : +10% C_D : +10% $C_{c,D}$: +10%	7.27	17.52
C_L : +10% C_D : +10% $C_{c,D}$: −10%	10.7	−21.28
C_L : +10% C_D : −10% $C_{c,D}$: −10%	8.52	3.42
C_L : −10% C_D : −10% $C_{c,D}$: −10%	9.84	−11.54
C_L : −10% C_D : +10% $C_{c,D}$: +10%	4.34	50.81
C_L : −10% C_D : −10% $C_{c,D}$: +10%	8.02	9.06
C_L : +10% C_D : −10% $C_{c,D}$: +10%	12.22	−38.39
C_L : −10% C_D : +10% $C_{c,D}$: −10%	7.67	13.05

The Monte Carlo simulation results of the pitch and yaw angles are shown in Figures 16 and 17, respectively. It can be observed that all the variables are within reasonable ranges with

smooth shapes. This is an illustration of the dynamic robustness to diverse uncertainties and the adaptability to attenuate disturbances.

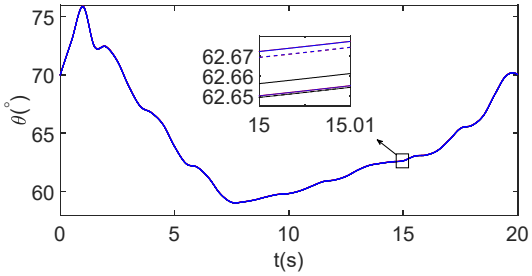

Figure 16. Pitch angle in the Monte Carlo simulation.

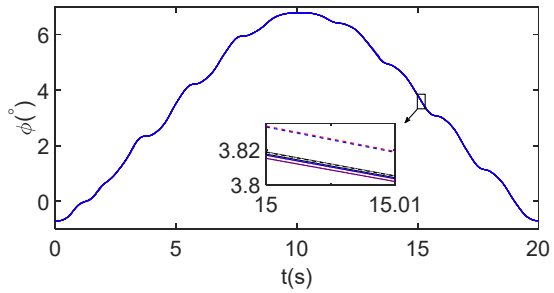

Figure 17. Yaw angle in the Monte Carlo simulation.

6. Conclusions

In this paper, the trajectory of the parafoil at high altitudes was optimized and tracked in a comprehensively parameterized manner. The PSM was employed to reformulate the original dynamic trajectory optimization problem into a static NLP problem, which could be solved by using an efficient sequential quadratic problem solver. The constraints of the state variables, control signals and boundary conditions were considered to make the optimized trajectory reasonable and smooth. The mature and reliable toolbox of Matlab can be used to solve the PSM optimization problem directly. The parameterized results can then be obtained, which is easy to code. To facilitate the implementation, a PID type linear time-invariant controller based on an extended state observer was developed to deal with the strong nonlinear dynamics directly.By doing so, there is no difference between linear and nonlinear dynamics when using this type of observer. Therefore, we can extend the application range of linear controllers to a wider kind of nonlinear dynamics. This is quite appealing for practitioners. The simulation results demonstrated the effectiveness of the proposed comprehensive optimization and control schemes.

Author Contributions: Methodology, software, writing—original draft preparation, X.L.; writing—review and editing, funding acquisition and supervision, M.S.; writing—review and editing, M.P., Z.C. All authors have read and agreed to the published version of the manuscript.

Funding: This work was supported by the National Natural Science Foundation of China [grant number 62073177, 61973175, 51777013].

Institutional Review Board Statement: Not applicable.

Informed Consent Statement: Not applicable.

Data Availability Statement: The data that support the findings of this study are available from the corresponding author upon reasonable request.

Conflicts of Interest: The authors declare no conflict of interest.

References

1. Cao, Y.; Hu, Q.; Shi, H.; Zhang, Y. Prediction of wind power generation base on neural network in consideration of the fault time. *IEEE Trans. Electr. Electron. Eng.* **2019**, *14*, 670–679. [CrossRef]
2. Archer, C.L.; Caldeira, K. Global assessment of high-altitude wind power. *Energies* **2009**, *2*, 307–319. [CrossRef]
3. Mondal, A.K.; Mondal, S.; Devalla, V.; Sharma, P.; Gupta, M.K. Advances in floating aerogenerators: Present status and future. *Int. J. Precis. Eng. Manuf.* **2016**, *17*, 1–12. [CrossRef]
4. Kim, J.; Park, C. Wind power generation with a parawing on ships, a proposal. *Energy* **2009**, *35*, 336–342.
5. Ran, X.L. *Study of Dynamics and Control on High Altitude Wind Power Generation Towing Parafoil*; National University of Defense Technology: Changsha, China, 2012.
6. Liu, Y.G.; Wang, Y.K.; Wan, Z.Q.; Yan, D. Research progress and prospect of tethered floating wind energy generation technology. *Adv. Aeronaut. Sci. Eng.* **2021**, *12*, 36–43.
7. Cherubini, A.; Papini, A.; Vertechy, R.; Fontana, M. Airborne wind energy systems: A review of the technologies. *Renew. Sustain. Energy Rev.* **2015**, *15*, 1461–1476. [CrossRef]
8. Costello, S. Real-Time Optimization via Directional Modifier Adaptation, with Application to Kite Control. Ph.D. Dissertation, EPFL, Lausanne, Switzerland, 2015.
9. Loyd, M.L. Crosswind kite power. *J. Energy* **1980**, *4*, 106–111. [CrossRef]
10. Zgraggen, A.U.; Fagiano, L.; Morari, M. On real-time optimization of airborne wind energy generators. In Proceedings of the 52nd IEEE Conference on Decision and Control (CDC), Florence, Italy, 10–13 December 2013; pp. 385–390.
11. Zgraggen, U.; Fagiano, L.; Morari, M. Real-time optimization and adaptation of the crosswind flight of tethered wings for airborne wind energy. *IEEE Trans. Control Syst. Technol.* **2015**, *23*, 434–448. [CrossRef]
12. Williams, P.; Lansdorp, B.; Ockesl, W. Optimal crosswind towing and power generation with tethered kites. *J. Guid. Control Dyn.* **2008**, *31*, 81–93. [CrossRef]
13. Ilzhofer, A.; Houska, B.; Diehl, M. Nonlinear MPC of kites under varying wind conditions for a new class of large-scale wind power generators. *Int. J. Robust Nonlinear Control* **2007**, *17*, 1590–1599. [CrossRef]
14. Canale, M.; Fagiano, L.; Milanese, M. High altitude wind energy generation using controlled power kites. *IEEE Trans. Control Syst. Technol.* **2010**, *18*, 279–293. [CrossRef]
15. Song, J.; Zhao, K.; Weng, H.; Huang, X.; Liu, Y. Research on reliable path planning of manipulator based on artificial beacons. In Proceedings of the 2019 IEEE International Conference on Dependable, Autonomic and Secure Computing, International Conference on Pervasive Intelligence and Computing, International Conference on Cloud and Big Data Computing, International Conference on Cyber Science and Technology Congress, Fukuoka, Japan, 5–8 August 2019.
16. Elnagar, G.; Kazemi, M.A.; Razzaghi, M. The pseudospectral Legendre method for discretizing optimal control problems. *IEEE Trans. Autom. Control* **1995**, *40*, 1793–1796. [CrossRef]
17. Gong, Q.; Fahroo, F.; Ross, I.M. Spectral algorithm for pseudospectral methods in optimal control. *J. Guid. Control Dyn.* **2008**, *31*, 460–471. [CrossRef]
18. Hu, W.J.; Lu, Q.; Chang, J. A Gauss pseudospectral method for reentry trajectory planning with characteristic trend partitioning. *Acta Aeronaut. Astronaut. Sin.* **2015**, *36*, 3338–3348.
19. Chen, H.; Fang, Y.C.; Sun, N.; Qian, Y.Z. Pseudospectral method based on time optimal anti-swing trajectory planning for double pendulum crane systems. *Acta Autom. Sin.* **2016**, *42*, 153–160.
20. Zhang, Y.B.; Zong, Q.; Lu, H.C. Formation trajectory optimization of quadrotor UAV based on HP adaptive pseudospectral method. *Sci. China Technol. Sci.* **2017**, *3*, 239–248.
21. Erhard, M.; Strauch, H. Control of towing kites for seagoing vessels. *IEEE Trans. Control Syst. Technol.* **2013**, *21*, 1629–1640. [CrossRef]
22. Fagiano, L.; Zgraggen Morari, M.; Khammash, M. Automatic crosswind flight of tethered wings for airborne wind energy: Modeling, control design, and experimental results. *IEEE Trans. Control Syst. Technol.* **2014**, *22*, 1433–1447.
23. Li, H.; Olinger, D.J.; Demetriou, M.A. Attitude tracking control of an airborne wind energy system. In Proceedings of the 2015 European Control Conference (ECC), London, UK, 11–14 July 2015; pp. 1510–1515.
24. Jiang, B.P.; Hamid, R.K.; Yang, S.C.; Gao, C.C.; Kao, Y.G. Observer-based adaptive sliding mode control for nonlinear stochastic Markov jump systems via T-S fuzzy modeling: Applications to robot arm model. *IEEE Trans. Ind. Electron.* **2020**, *99*, 1. [CrossRef]
25. Han, J.Q. From PID to active disturbance rejection control. *IEEE Trans. Ind. Electron.* **2009**, *56*, 900–906. [CrossRef]
26. Gao, Z.Q. Scaling and bandwidth-parameterization based controller tuning. In Proceedings of the American Control Conference, Denver, CO, USA, 4–6 June 2003; pp. 4989–4996.
27. Huang, Y.; Xue, W.C. Active disturbance rejection control: Methodology and theoretical analysis. *ISA Trans.* **2014**, *53*, 963–976. [CrossRef] [PubMed]
28. International Towing Tank Conference: ITTC Symbols and Terminology List Version 2014, September 2014. Available online: http://ittc.info/media/4004/structured-list2014.pdf (accessed on 16 May 2021).